Available online at www.sciencedirect.com
SCIENCE DIRECT®
ELSEVIER
Nuclear Physics A 714 (2003) 3–20
NUCLEAR PHYSICS A
www.elsevier.com/locate/npe

^{100}Mo$(\vec{p}, d)^{99}$Mo reaction at 21 MeV and direct reaction analysis of the low-lying continuum spectrum

S. Hirowatari [a], Syafarudin [a,*], F. Aramaki [a], A. Nohtomi [a,1], G. Wakabayashi [a], Y. Uozumi [a], N. Ikeda [a], M. Matoba [a] Y. Aoki [b], K. Hirota [b], N. Okumura [b], T. Joh [b]

[a] *Department of Nuclear Engineering, Kyushu University, Fukuoka 812-8581, Japan*
[b] *Tandem Accelerator Center, Tsukuba University, Tsukuba 305-8577, Japan*

Received 11 April 2002; received in revised form 2 October 2002; accepted 18 October 2002

Abstract

The ^{100}Mo$(\vec{p}, d)^{99}$Mo reaction has been studied with 21 MeV polarized protons. Momentum spectra of the emitted deuterons corresponding to the excitation energy region up to 5.75 MeV in ^{99}Mo have been measured. Theoretical analysis based on the standard distorted-wave Born approximation (DWBA) provides the lj-angular momentum transfers and spectroscopic factors of neutron hole states for 27 levels from the ground state up to $E_X = 2.921$ MeV. The polarization data gave a more affirmative information in assigning the spins and parities. Spectrum regions from discrete levels to continuum were treated with a global analysis using the direct reaction model and continuous strength functions. The double differential cross section-energy spectra were reproduced fairly well using the DWBA-based cross sections and the asymmetrical Lorentzian form strength response function having energy-dependent spreading widths.

PACS: 24.10.-i; 21.10.Jx; 21.10.Pc

Keywords: Low-lying continuum, (polarized p, d) reaction, $E_p = 65$ MeV; measured $\sigma(E, \theta)$, $A_y(E, \theta)$; ^{99}Mo deduced levels, l, j; Spectroscopic factors; DWBA analysis

* Corresponding author.
E-mail address: safar@nucl.kyushu-u.ac.jp (Syafarudin).
[1] Present address: Proton Medical Research Center, University of Tsukuba, Tsukuba 305-8575, Japan.

0375-9474/02/$ – see front matter
PII: S0375-9474(02)01353-2

1. Introduction

One can observe a low-lying continuum spectrum in the one-nucleon transfer reactions by means of medium-weight mass target nuclei and moderate bombarding enegies, i.e., just above the region where discrete excitation levels are mainly populated [1]. The spectrum is found to be structured discretely and in a complicated way at the excitation energy of several MeV, then gradually becomes structureless as it comes to the higher area, and finally forms a plateau. Such an appearance of a spectrum is understood as a reflection of the phenomena occured in shell-orbits, e.g., nuclear damping, shell-orbit fragmentation, nuclear surface vibration.

In some previous studies [2–7], the empirical strength response functions of major shell-orbits in the nucleus have been extracted. All the results are in accord in indicating the wide fragmentation of deeply bound states. As a matter of fact, the effect of nucleon pickup and direct reaction originating in deeper shell-orbits, plays an important role in configuring the spectrum below a couple of ten MeV, more contributive than any other effect such as compound and multi-step reactions. However, it is difficult to separate the contribution of the cross section due to direct reaction from the other contributions experimentally; the spectrum can be analyzed on the whole as a summative result of amplitudes of multi-shell-orbits. Therefore, an approach such as proposed by Lewis [8] is suggested to be employed, in parallel with the prediction models described by Crawley [9] and Galès et al. [10], to analyze such a continuum in a systematic way.

In agreement with Lewis, Matoba et al. [11,12] have advanced an analysis using an asymmetrical Lorentzian shaped strength function having energy-dependent spreading widths and DWBA-based cross sections, to describe the reaction process ruling the low-lying spectrum. This method has been applied successfully to the $2p$–$1f$ shell nuclei, by means of the $(\vec{p}, d)$ reactions on ^{48}Ca and ^{58,60,62,64}Ni targets at $E_p = 65$ MeV [13,14]. Nevertheless, it is interesting to investigate the generality of the method in extensive target nuclei and projectile energy regions.

The present paper describes results of studies on the ^{100}Mo$(p, d)^{99}$Mo reaction experiment with 21 MeV polarized protons. The series of Mo-isotopes is a good example to discuss the nuclear structure models of the $3s$–$1g$ shell nuclei, and ^{99}Mo is one of the heavier Mo-isotopes to be investigated for detailed level structure. In order to achieve a more comprehensive understanding toward the low-lying continuum, at first, the assignment of excitation levels in the region of 0–2.921 MeV was carried out. Using the vector analyzing powers of the ^{100}Mo$(p, d)^{99}$Mo reaction the spins and parities of 27 levels were determined. The derived results were compared with those previously observed by Bindal et al. [15], as well as by Firestone et al. [16]. Finally, the spectrum was analyzed systematically using a continuous strength function and DWBA-based cross sections of the correlated neutron hole states.

2. Experiment

2.1. Experimental procedure

The experiment was carried out at the Tandem Accelerator Center, University of Tsukuba. A polarized proton beam with the polarization of about 80% accelerated to the energy of 21 MeV was used. The beam was bombarded onto an enriched (97.27%) ^{100}Mo target foil with a thickness of 0.505 mg/cm^2. The beam intensity ranged between 40 and 200 nA. Emitted deuterons were detected by the focal plane of an ESP-90 spectrograph with a position-sensitive proportional counter (PSPC) detector system [17,18]. Angular distributions of cross sections and analyzing powers were measured at $8^\circ \sim 68^\circ$ ($12^\circ \sim 68^\circ$ for higher excitation energy region) laboratory angles. The measured energy range corresponds to the excitation energy region from the ground state to about 6 MeV. The next region could not be measured because of a considerable 'contaminant' due to elastic protons appearing in the same momentum region, which was verified from the obvious deviation from typical resolution, and the peak movement of different scattering angles. Such kind of contaminant was not found in the region below 6 MeV. The normalization of the cross section was performed by scaling the measured $p + {}^{100}$Mo elastic scattering cross section to an optical model prediction using parameters of global potentials [19].

2.2. Experimental results

Fig. 1 shows a typical spectrum of emitted deuterons from the ^{100}Mo$(p, d)^{99}$Mo reaction with $E_p = 21$ MeV at 20° laboratory angle. The obtained spectrum region corresponds to the excitation energy up to 6 MeV in ^{99}Mo. Due to the doubtfulness on the high energy side, the region of experimental data to analyze was limited below the excitation energy of 5.75 MeV. The energy calibration of the spectrum was performed by remapping some positions—which was done by adjusting the strength of the magnetic field—of well-known low-lying levels in ^{99}Mo, namely ground state, 0.0978, 0.2355, 0.3512 and 0.6150 MeV [16], over a wide region in the spectrum. From the relationship between the positions and curvature radii of the deuteron at some values of the magnetic field, a general formulation of energy calibration was obtained. Furthermore, the calibration was fine-tuned using a linear function to optimize the errors attributed to run-to-run variations of integrated beam current, which were estimated to be of the order of a few percentages. The resultant energy resolution on the experimental spectrum was about 50 keV (in FWHM) for the region above ~ 2 MeV, and better than 40 keV for the lower region, which is considered mainly due to the resolutions of beam, the PSPC detector and the existence of background.

A group of discrete levels are populated throughout the region up to about 3 MeV, and the strongly excited states are almost all in the region below 2 MeV. The continuum spectrum region is found to exist in the relatively lower area starting from about 2 MeV. The peaks were extracted from the spectrum using a peak fitting and peeling-off code that can provide data reduction good for a maximum of four peaks at a time. However, of unconvenience, it is not desirable to fit all the peaks at a time, since the peak-widths (FWHMs) observed in the spectrum change as a function of the excitation energy and/or

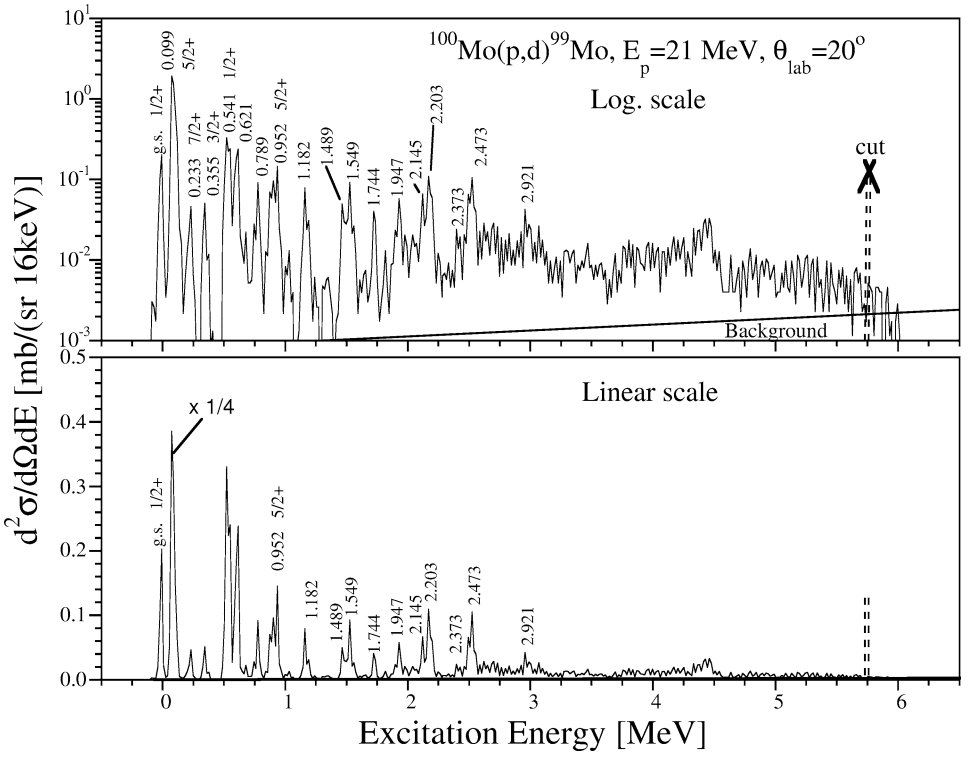

Fig. 1. A typical energy spectrum of deuterons emitted from the ^{100}Mo$(p,d)^{99}$Mo reaction at 21 MeV in log. scale (top) and linear scale (bottom).

the position on the PSPC detector. Then, we used single search-parameter for all the peak-widths in a comparatively narrow region. Namely, peaks at 0.541, 0.621, 0.686, and 0.789 MeV should be extracted together since the peak at 0.686 MeV is almost covered by the other peaks and is too weak to own its resolution without referring to the neighbor peaks. Similarly for the peaks in the region above 2 MeV, the region was partitioned in groups with 2 to 4 peak-elements so that each group can be approached with single parameter of peak-resolution. The peaks populated in the region higher than 3 MeV were not analyzed because of the ambiguity of assignment, which was much masked by the background of continuum.

In the present analysis, the physical background in the deuteron spectra are treated as follows. For the discrete level analysis, the effects of nuclear damping of single-particle (hole) strength and the contributions from other reaction processes than direct ones are treated as background. The background lines were drawn consistently using a slight-sloping exponential function of $C_0 e^{\alpha E_x}$ starting from ground state up to 6 MeV (Fig. 1), where C_0 and α are constants. The background subtraction procedure affects slightly the data of the peaks located in the region $E_x \geqslant 1.5$ MeV. For the continuum spectrum analysis, all the above-mentioned contributions are included in the spectrum to analyze as a part of single-particle (hole) spectroscopic strengths.

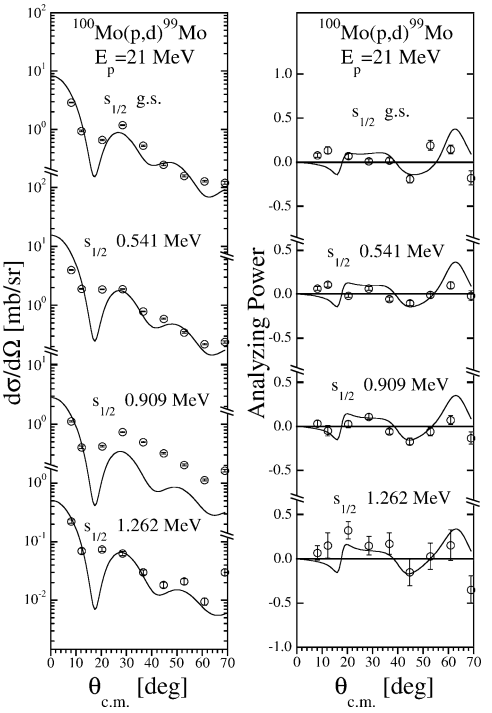

Fig. 2. Angular distributions for cross section (left) and analyzing power (right) for $1/2^+$ transitions in the ^{100}Mo$(p,d)^{99}$Mo reaction at 21 MeV. The solid curves show the DWBA predictions.

Angular distributions for the analyzed excitation levels are shown in Figs. 2–8 together with the predictions of the DWBA theory using the optical potential parameters set listed in Table 1 for the ^{100}Mo$(p,d)^{99}$Mo reaction at 21 MeV, as described in the next section. From comparisons between the experimental and theoretical angular distributions of cross sections and analyzing powers, the lj-angular momentum transfers were assigned.

Thirty-two levels were analyzed in the excitation energy region below 3 MeV, and the lj-transfers were assigned for 27 levels. In some cases, angular distributions of the cross sections and analyzing powers show such obscure oscillatory patterns that the assignments could not be done uniquely. The resultant data of the lj-transfers are summarized in Table 2 together with the results of Refs. [15,16] and the discussions can be seen in Section 4.1. As described in Section 4.2, the entire spectrum region from ground state up to continuum area is analyzed consistently by considering all the constituent shell-orbits in the concerned energy area.

3. Theoretical analysis

3.1. DWBA analysis for single-hole states

The differential cross section and analyzing power data were analyzed with the DWBA code DWUCK [20] based on the zero-range and local energy approximation model. The

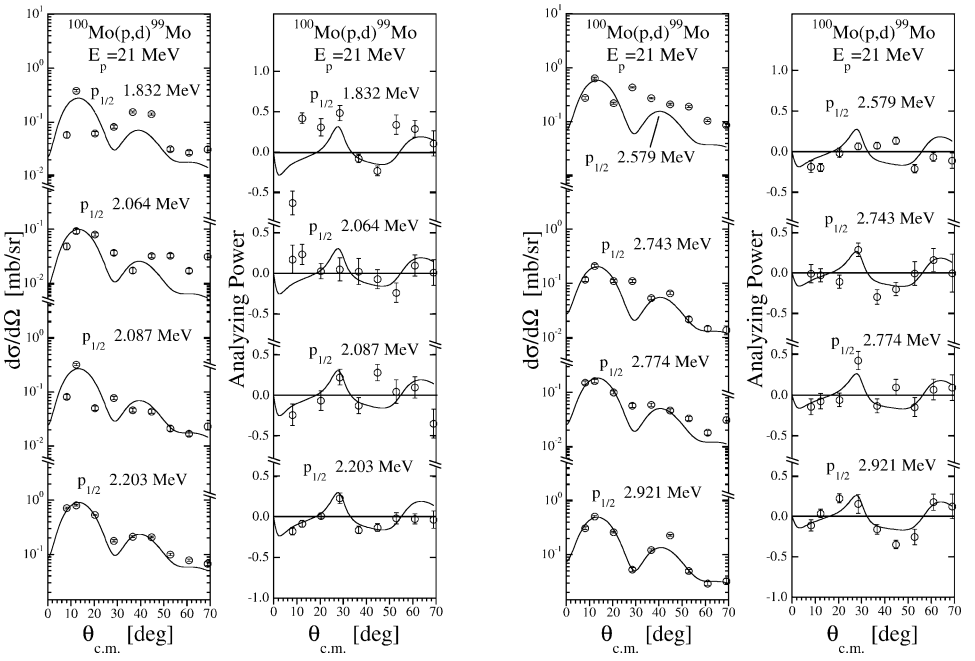

Fig. 3. Same as Fig. 2 for $1/2^-$ transitions.

neutron bound state wave functions were generated by using a Woods–Saxon well with the standard geometrical parameters $r_n = 1.25$ fm and $a_n = 0.65$ fm, including a Thomas–Fermi spin–orbit term with the usual $\lambda = 25$ factor. The well depth was adjusted to reproduce the neutron separation energy. In the local energy approximation model of DWBA, the parameter for the finite range effects was set to 0.621. Parameters of the non-locality effect for neutron, proton, and deuteron potentials, respectively, $\beta_n = 0.85$, $\beta_p = 0.85$, and $\beta_d = 0.54$, were adopted.

The use of an adiabatic potential constructed from the global potential of neutrons and protons [21] for the deuteron channel in the (p, d) reaction improves considerably the overall fitting of the angular distributions compared with conventional best-fit optical potentials for the elastic deuteron scattering. Hence, the adiabatic potential parameter was adopted for deuterons. While for protons, the global optical potential parameter of Becchetti and Greenlees [19] was used.

The spectroscopic factor for a single-hole state of (p, d) reaction then can be extracted using the following relation,

$$\frac{d\sigma}{d\Omega} = \left[\frac{2S_d + 1}{2S_p + 1}\frac{D_0^2}{1.0 \times 10^4}\right]\frac{C^2S}{2j+1}\left(\frac{d\sigma}{d\Omega}\Big|_{l,j}^{\mathrm{DW}}\right), \tag{1}$$

where, $S_p(= 1/2)$ is the proton spin, $S_d(= 1)$ is the deuteron spin, and $D_0^2(= 1.53 \times 10^4)$ is the constant of zero-range integration. C^2S, j, and $d\sigma/d\Omega|_{l,j}^{\mathrm{DW}}$ are, respectively, the spectroscopic factor, total angular momentum transfer, and resultant DWBA differential

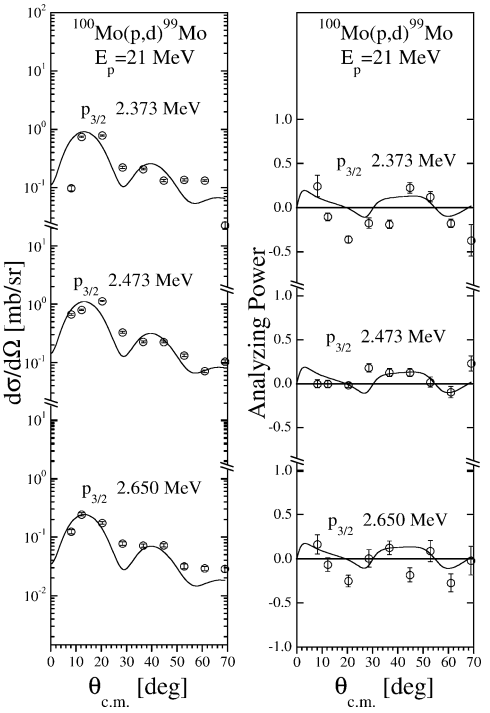

Fig. 4. Same as Fig. 2 for $3/2^-$ transitions.

cross section due to the code DWUCK [20]. The recommended value 2.30 is used as the result of the term in the square brackets in Eq. (1).

3.2. Incoherent sum of DWBA calculations

Double differential cross sections are analyzed with the direct reaction model composed by an incoherent sum of the DWBA predictions from all the constituent shell-orbits, as expressed by

$$\frac{d^2\sigma}{d\Omega\, dE} = 2.30 \sum_{l,j} \left[\frac{C^2 S_{l,j}(E)}{2j+1} \times \left(\frac{d\sigma}{d\Omega} \Big|^{\mathrm{DW}}_{l,j}(E) \right) \right], \tag{2}$$

where $d\sigma/d\Omega|^{\mathrm{DW}}_{l,j}(E)$ is the DWBA cross section. $C^2S_{l,j}(E)$ is the function of spectroscopic strength for the lj-transfer, given as follows

$$C^2 S_{l,j}(E) = \left(\sum C^2 S_{l,j} \right) \times f_{l,j}(E). \tag{3}$$

We used the values of spreading widths to estimate the imaginary parts of the bound state potential discussed in Refs. [22,23]. The strength distribution is estimated by an asymmetrical Lorentzian function [11,12,22] as follows.

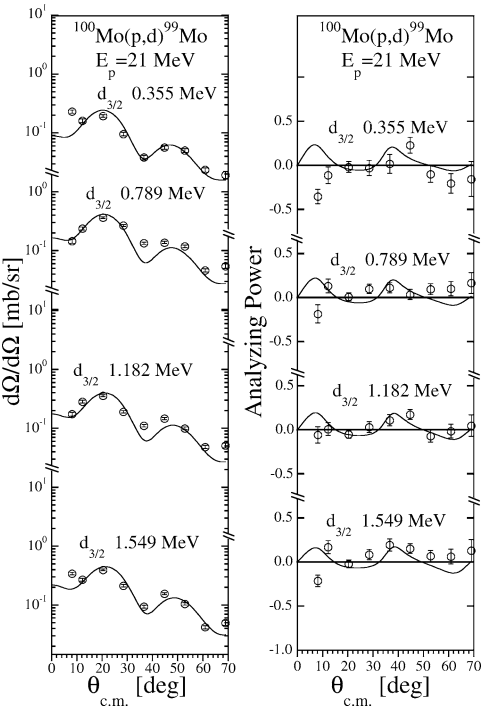

Fig. 5. Same as Fig. 2 for $3/2^+$ transitions.

$$f_{l,j}(E) = \frac{n_0}{2\pi} \frac{\Gamma(E)}{(|E - E_F| - E_{l,j})^2 + \Gamma^2(E)/4}, \tag{4}$$

$$\int_0^\infty f_{l,j}(E)\, dE = 1, \tag{5}$$

where $E_{l,j}$ is the calculated energy of the single-particle state which varies with the spreading width $\Gamma(E)$, and n_0 is the normalization constant deduced from a shell-model calculation. The sum-rule fraction of spectroscopic factors $C^2 S_{l,j}$ and the centroid energies for $j = l \pm \frac{1}{2}$ shell-orbits are estimated by using the BCS-theory, and the single-particle energies are calculated based on a prescription shown in Ref. [24]. The energy variable is taken as E–E_F in consistency with the work of Hisamochi et al. in Ref. [6].

The spreading width is fairly well expressed with a function proposed by Brown and Rho [25], as well as by Mahaux and Sartor [22], as

$$\Gamma(E) = \frac{\epsilon_0 (E - E_F)^2}{(E - E_F)^2 + E_0^2} + \frac{\epsilon_1 (E - E_F)^2}{(E - E_F)^2 + E_1^2}, \tag{6}$$

where ϵ_0, ϵ_1, E_0, and E_1 are constant parameters to express the effects of nuclear damping. The first term in Eq. (6) corresponds just to the general trend of the infinite Fermi gas model prediction [26], with saturation characteristics at the $E \to \infty$ limit, and the second term

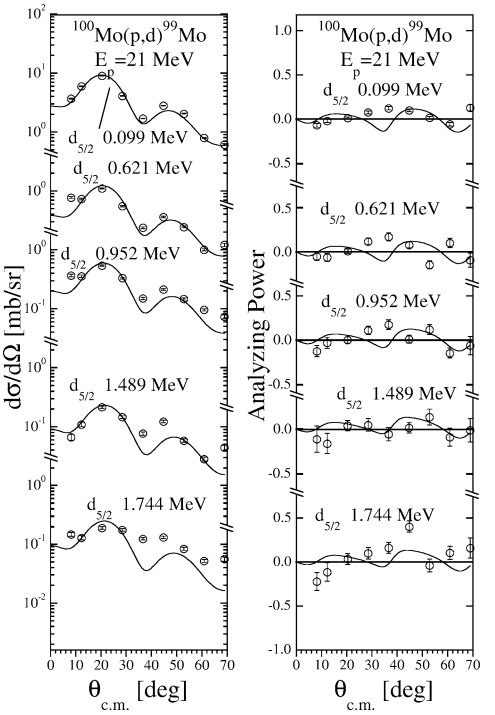

Fig. 6. Same as Fig. 2 for $5/2^+$ transitions.

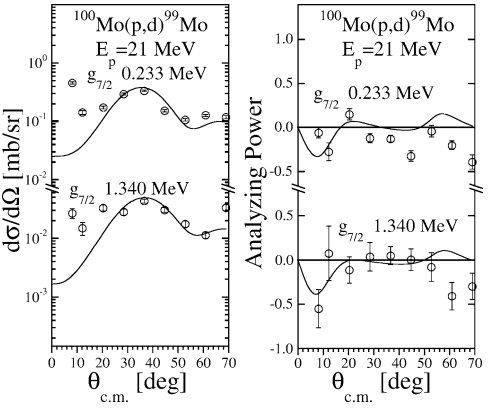

Fig. 7. Same as Fig. 2 for $7/2^+$ transitions.

corresponds to the existence of an additional onset of the nuclear damping near the Fermi surface. The estimated parameters [11,12] are given as follows:

$$\epsilon_0 = 19.4\ (\text{MeV}), \qquad E_0 = 18.4\ (\text{MeV}),$$
$$\epsilon_1 = 1.40\ (\text{MeV}), \qquad E_1 = 1.60\ (\text{MeV}). \tag{7}$$

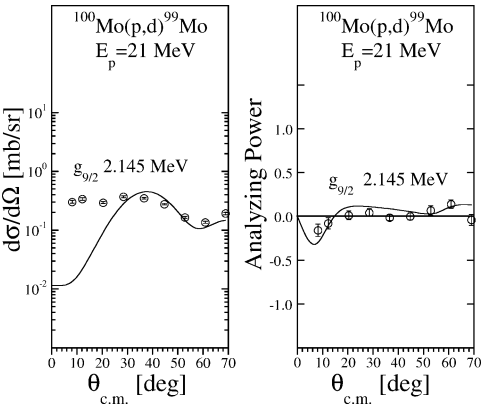

Fig. 8. Same as Fig. 2 for $9/2^+$ transitions.

Table 1
Optical model parameters used in the DWBA calculations for ^{100}Mo$(p,d)^{99}$Mo reaction at 21 MeV

Particle	V (MeV)	r (fm)	a (fm)	r_c (fm)	W_v (MeV)	W_s (MeV)	r' (fm)	a' (fm)	V_{so} (MeV)	r_{so} (fm)	a_{so} (fm)
proton	54.74	1.17	0.75	1.25	1.92	8.47	1.32	0.62	6.20	1.01	0.75
deuteron	[a]	1.17	0.78	1.25	[b]	[b]	1.29	0.63	6.20	1.06	0.75
neutron	[c]	1.25	0.65			Spin orbit term		$\lambda = 25$			

	Non-locality parameters (fm)	Finite-range parameter (fm)
proton	0.85	0.621
neutron	0.85	
deuteron	0.54	

[a] $V = 110.3 - 0.64(E_d/2) + 0.4Z/A^{1/3}$ (MeV).
[b] $W_v = 0.44(E_d/2) - 4.26$ (MeV), $W_s = 24.8 - 0.50(E_d/2)$ (MeV), E_d is the deuteron kinetic energy.
[c] Well depth adjusted to fit the separation energy.

The sum-rules of the spectroscopic factors of nucleon orbits for $T \pm \frac{1}{2}$ isospin states above the closed shell core are estimated with a simple shell model prescription [27] as described in the following equation:

$$\sum C^2 S_{l,j} = \begin{cases} n_{n(l,j)} - \dfrac{n_{p(l,j)}}{2T+1}, & \text{for } T_< = T - \frac{1}{2}, \\ \dfrac{n_{p(l,j)}}{2T+1}, & \text{for } T_> = T + \frac{1}{2}. \end{cases} \tag{8}$$

Here, $n_{n(l,j)}$ and $n_{p(l,j)}$, respectively are the numbers of neutrons and protons in the shell-orbit concerned, and T is the isospin of the target nucleus.

Table 2
Spectroscopic results from neutron pickup reactions on ^{100}Mo

No.	Present work				Ref. 1[a]					Ref. 2[b]	
	$E_x \pm \delta E_x$ ($\mathrm{MeV}_{\mathrm{keV}}$)	l	j^π	C^2S $(\vec{p},d)$	E_x (MeV)	l	j^π	C^2S (p,d)	C^2S (d,t)	E_x (MeV)	j^π
1	0.000	0	$\frac{1}{2}^+$	0.15	0.000	0	$\frac{1}{2}^+$	(0.30)	0.14	0.000	$\frac{1}{2}^+$
2	0.099_{2}	2	$\frac{5}{2}^+$	1.90	0.098	2	$\frac{5}{2}^+$	1.84	1.80	0.098	$\frac{5}{2}^+$
3	0.233_{5}	4	$\frac{7}{2}^+$	1.32	0.231	4	$\frac{7}{2}^+$	1.39	1.75	0.236	$\frac{7}{2}^+$
4	0.355_{7}	2	$\frac{3}{2}^+$	0.07	0.345	2	$\frac{3}{2}^+$	0.06	0.16	0.351	$\frac{3}{2}^+$
5	0.541_{15}	0	$\frac{1}{2}^+$	0.19	0.531	0	$\frac{1}{2}^+$			0.525	$\frac{1}{2}^+$
6						2	$\frac{3}{2}^+$	0.33	0.55	0.549	$\frac{3}{2}^+$
7	0.621_{20}	2	$(\frac{5}{2}^+)$	(0.30)	0.604	2	$\frac{5}{2}^+$	0.24	0.32	0.615	$\frac{5}{2}^+$
8										0.632	$\frac{3}{2}^+$
9	0.686_{17}				0.675	5	$\frac{11}{2}^-$	0.50	(1.20)	0.698	$(\frac{7}{2}^+)$
10					0.747	2	$\frac{5}{2}^+$	0.07	0.10	0.754	$\frac{7}{2}^+$
11	0.789_{9}	2	$\frac{3}{2}^+$	0.13	0.788	(2)	$(\frac{3}{2}^+)$	0.06	0.08	0.793	$(\frac{3}{2},\frac{5}{2})^+$
12					0.878	(2)	$(\frac{3}{2}^+)$	0.07	0.06	0.890	$\frac{3}{2}^+$
13	0.909_{15}	0	$\frac{1}{2}^+$	0.06		(4)	$(\frac{9}{2}^+)$	0.59	0.30	0.906	$\frac{1}{2}^+$
14	0.952_{15}	2	$\frac{5}{2}^+$	0.16	0.924	2	$\frac{5}{2}^+$	0.15	0.22	0.945	$\frac{5}{2}^+$
15	1.047_{23}				1.022	(3)	$(\frac{5}{2}^-)$	0.26		1.026	$(\frac{3}{2}^+,\frac{5}{2}^+)$
16	1.182_{17}	2	$\frac{3}{2}^+$	0.15	1.165	2	$\frac{5}{2}^+$	0.10	0.08	1.167	$\frac{5}{2}^+$
17										1.196	
18										1.198	$\frac{3}{2}^+$
19	1.262_{27}	0	$\frac{1}{2}^+$	0.01						1.280	
20	1.340_{28}	4	$\frac{7}{2}^+$	0.25	1.320	4	$\frac{7}{2}^+$	0.10			
21	1.382_{12}									1.383	$\frac{3}{2}^+,\frac{5}{2}^+$
22										1.442	$(\frac{3}{2},\frac{5}{2})^+$
23	1.489_{36}	2	$\frac{5}{2}^+$	0.08	1.455	2	$\frac{3}{2}^+$	0.10	0.10	1.494	$\frac{5}{2}^+$
24	1.549_{36}	2	$\frac{3}{2}^+$	0.20	1.516	2	$\frac{3}{2}^+$	0.13	0.15	1.561	$\frac{1}{2}^+,\frac{3}{2},\frac{5}{2}^+$
25										1.571	$\frac{1}{2},\frac{3}{2},\frac{5}{2}^+$
26					1.637	5	$\frac{11}{2}^-$	0.07			
27										1.682	$(\frac{3}{2}^+,\frac{5}{2}^+)$
28	1.744_{36}	2	$\frac{5}{2}^+$	0.08	1.714	2	$\frac{3}{2}^+$	0.05	0.05		
29					1.793	4	$\frac{7}{2}^+$	0.17	0.10		
30	1.832_{38}	1	$\frac{1}{2}^-$	0.06	1.891	1	$\frac{1}{2}^-$	0.12	0.11	1.893	$(\frac{1}{2}^-,\frac{3}{2}^-)$
31	1.947_{38}				1.910	1	$\frac{1}{2}^-$	0.27			
32					1.934	4	$\frac{9}{2}^+$	0.19			
33	2.064_{50}	1	$\frac{1}{2}^-$	0.03							
34	2.087_{50}	1	$\frac{1}{2}^-$	0.07							

(*continued on next page*)

Table 2 (*Continued*)

No.	Present work				Ref. 1[a]					Ref. 2[b]	
	$E_x \pm \delta E_x$ ($\mathrm{MeV_{keV}}$)	l	j^π	C^2S $(\vec{p},d)$	E_x (MeV)	l	j^π	C^2S (p,d)	(d,t)	E_x (MeV)	j^π
35	2.145_{50}	4	$\frac{9}{2}^+$	1.65	2.103	4	$\frac{9}{2}^+$	1.02	1.00		
36	2.203_{50}	1	$\frac{1}{2}^-$	0.24	2.155	1	$\frac{1}{2}^-$	0.28	0.26		
37	2.373_{50}	1	$\frac{3}{2}^-$	0.23	2.330	2	$\frac{3}{2}^+$	0.06	1.00		
38	2.473_{50}	1	$\frac{3}{2}^-$	0.30	2.436	1	$\frac{1}{2}^-$	0.24	0.20		
39	2.579_{50}	1	$\frac{1}{2}^-$	0.18	2.531	1	$\frac{1}{2}^-$	0.10			
40	2.650_{50}	1	$\frac{3}{2}^-$	0.07	2.591	1	$\frac{1}{2}^-$	0.09			
41	2.743_{50}	1	$\frac{1}{2}^-$	0.07	2.632	1	$\frac{1}{2}^-$	0.13			
42	2.774_{50}	1	$\frac{1}{2}^-$	0.06	2.702	1	$\frac{1}{2}^-$	0.10			
43	2.847_{50}				2.797	2	$\frac{5}{2}^+$	0.04			
44	2.921_{50}	1	$\frac{1}{2}^-$	0.18	2.870	1	$\frac{1}{2}^-$	0.17			

[a] Unpolarized beam experiment [15].
[b] Table of isotope [16].

4. Discussion

4.1. Low-lying level structure in ^{99}Mo and DWBA analysis

Angular distributions of cross sections and analyzing powers for 27 levels assigned for laboratory angles from 5° to 68° are shown in Figs. 2–8, along with the DWBA predictions. Since a low bombarding energy was used in the present experiment, the resultant analyzing powers are found to be somewhat structureless, so that it is difficult to distinguish j values from the weakly excited states having the same l-transfer.

The spins and parities of the ground state, the 0.541, 0.909, 1.262 MeV states for $1/2^+$ (Fig. 2), the 2.203, 2.921 MeV states for $1/2^-$ (Fig. 3), the 0.099 MeV state for $5/2^+$ (Fig. 6), and the 2.145 MeV state for $9/2^+$ (Fig. 8) were assigned unambiguously. The assignment results on these levels excluding the 0.541, 0.909 and 1.262 MeV states, are in good agreement with those of Bindal et al. [15] for both spin-parities and spectroscopic factors. The levels at 1.832, 2.064, 2.087, 2.579, 2.743, and 2.774 MeV, as well as the levels at 2.373, 2.473, and 2.650 MeV were assigned as $l = 1$ transfer, which could be confirmed from the analyzing powers as $1/2^-$ and $3/2^-$ states, respectively (Figs. 3, 4). Taking into account the most credible pattern of $5/2^+$ at 0.099 MeV, the levels at 0.952, 1.489, and 1.744 MeV could be assigned as $5/2^+$ states (Fig. 6). Four levels at 0.355, 0.789, 1.182, and 1.549 MeV were also assigned as $l = 2$ transfer, and using the characteristic of analyzing powers, they were distinguished as $3/2^+$ states (Fig. 5). We also could assign the levels at 0.233 and 1.340 MeV as $7/2^+$ states (Fig. 7). However, due to the complexity and a mixed region, no assignment has been done for the other excited levels higher than 2.921 MeV.

From Table 2, it is understood that the energy levels, spin-parities, and spectroscopic factors of low-lying levels determined in the present work are almost in reasonable

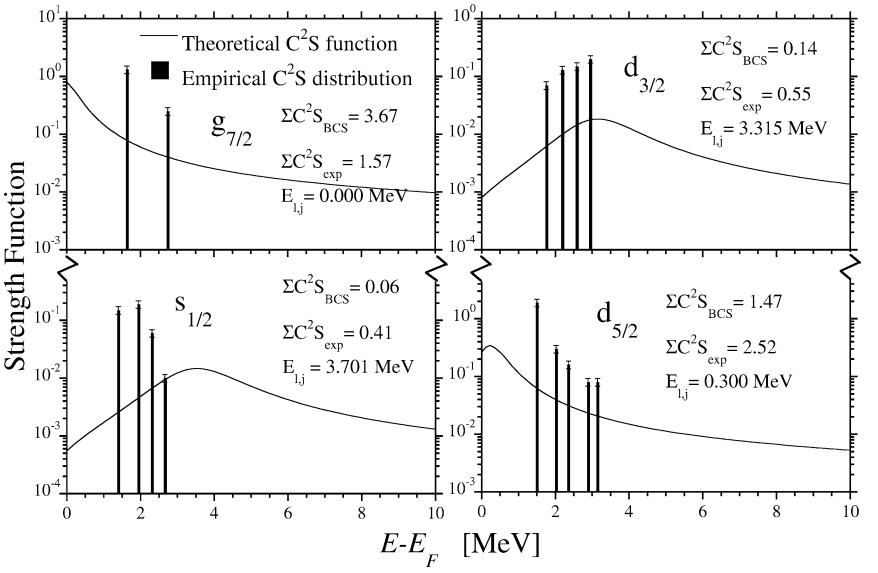

Fig. 9. Comparisons between the theoretical strength function and 'empirical' strength distribution of the $7/2^+$, $5/2^+$, $3/2^+$ and $1/2^+$ shell-orbits in ^{99}Mo. Theoretical centroid energies were estimated by the BCS-theory. $E_{l,j}$ in the figure refers to the theoretical value.

agreement with Bindal et al. [15] and with the table of isotopes Ref. [16]. Since the polarized beam was used in the present experiment, the spin and parity assignment should be more reliable than those in previous works. Since the usual definition of D_o^2 values for DWBA analysis was used [16] in the present study, the normalization constant value of the DWBA analysis for the (p, d) reaction used in the present study was 2.30, i.e., 0.90 times smaller than that used by Bindal et al. (2.54).

It is understood from the present experimental result that the distributions of positive parity states in the excitation energy region of 0–2 MeV and negative parity states in 2–3 MeV are clarified definitely. The single-hole states of $j = l \pm \frac{1}{2}$ shell-orbits having the same j-transfer exist rather as mixtures even in the low excitation energy region in ^{99}Mo. The C^2S value for the ground state is 0.14, which agrees with a value from the (d, t) reaction, not with the (p, d) value by Bindal et al. The level at 0.621 MeV is assigned as $l = 2$ transfer from the angular distribution of the cross section, but the j value cannot be assigned in the present work. This state is possibly admixed with $3/2^+$ and $5/2^+$. In agreement with the table of isotopes Ref. [16] four other stationary peaks, i.e., levels at 0.686, 1.382, 1.947, and 2.847 MeV have been recognized. Nevertheless, since these levels are very weak, they could not be assigned uniquely in the present work.

4.2. Continuum spectrum in ^{99}Mo and approach with single-hole strength functions

Fig. 9 shows the comparisons between the experimental and BCS-theoretical strength functions. The prescription of Bohr & Mottelson [24] which is modified to fit the ^{40}Ca single-hole states deduced by Nedjadi et al. [28] was used to calculate the single-

particle energies. The isobaric analog ground state $E_{T_>}$ of ^{99}Mo is known as the level at 14.678 MeV. The values of Fermi energies for neutron $E_F(n)$ and proton $E_F(p)$, separation energies for neutron S_n and proton S_p of ^{100}Mo, respectively, -6.790 and -9.148, 8.291 and 11.133 MeV were used in the calculation. As understood from BCS calculation, only shell-orbits from $2p_{1/2}$ to $3s_{1/2}$ of $T_<$ should play an important role in forming the shape of the spectrum below 6 MeV, while the elements of $T_>$ do not at all. As shown in Fig. 9, the estimated values of centroid energies and total spectroscopic factors of the $3s_{1/2}$, $2d_{3/2}$, $2d_{5/2}$, and $1g_{7/2}$ shell-orbits are in poor agreement with the 'empirical' one, since, only a part of the constituent levels could be considered in the calculation of centroid energies. It is because the levels in the shell concerned ($N = 50 \sim 80$) severely entwine one another, as can be explained by the 'WS + OS' shell-model. In this case, the ambiguity due to the procedure of fitting theoretical values to experimental data, namely, the parameter 2.30 in Eqs. (1) and (2), is far more influential than the energy resolution. The procedure is estimated to generate the ambiguity of about 15% of the obtained spectroscopic factors. However, the discrepancies impinge on the microscopic shape of the spectrum, but they are effectless for the wide range cumulative cross section. It should be noted that the hole strengths observed by $(e, e'p)$ knockout reactions are depleted in about $40 \sim 50\%$ of the limit expected in a shell model prediction [29,30]. In the present work, the strength distribution is calculated using the BCS model with the energy-dependence of spreading width determined from experimental data and theoretical predictions [11]. Our previous results of the studies on (p, d) reactions show rather smaller depletion of about $10 \sim 20\%$ of the theoretical limit [11,12,31]. However, the analysis of (p, d) reaction data has a severe problem in the absolute normalization, and the depletion in observed hole strengths is still now an open problem.

In the present study, the measured energy spectra were analyzed with overlaps of the DWBA predictions as described in Section 3.2. The measured energy spectra of double differential cross sections and analyzing powers were converted to 500 keV wide energy spectra. Fig. 10 shows double differential energy spectra for laboratory angles of 20°–68°, with solid lines representing theoretical cross sections and analyzing powers, and histograms the experimental ones. The values of the analyzing powers of the summed spectra are generally small and the shapes are rather structureless, although those for many discrete levels in the lower excitation energy region are large and have definite structure as shown in Figs. 2–8. As understood from Fig. 10, the theory predicts fairly well the cross section value in the excitation energy region of 0–2 MeV, while it does not in the region above 2 MeV. For analyzing power spectra, theory predicts rather smaller values and structureless shapes in all the excitation energy regions, and these features compare reasonably to experiment. In case of the condition similar to the present reaction, since the analyzing powers for two spins and parities exhibit rather similar angular distributions, however of opposite sign, it is no surprise that an average over a large energy range results in a structureless distribution of vanishing size. The residual contributions, i.e., experimental values minus theoretical values, are also shown in Fig. 10 (left) as dashed lines. These curves may correspond to some contributions from non-pickup direct reaction processes, like FSI or few-step reaction processes.

In Fig. 11 (top and middle), the energy spectra are converted to angular distributions and summed up for the excitation energy regions of 0–2 and 2–5.75 MeV, i.e., the peak-

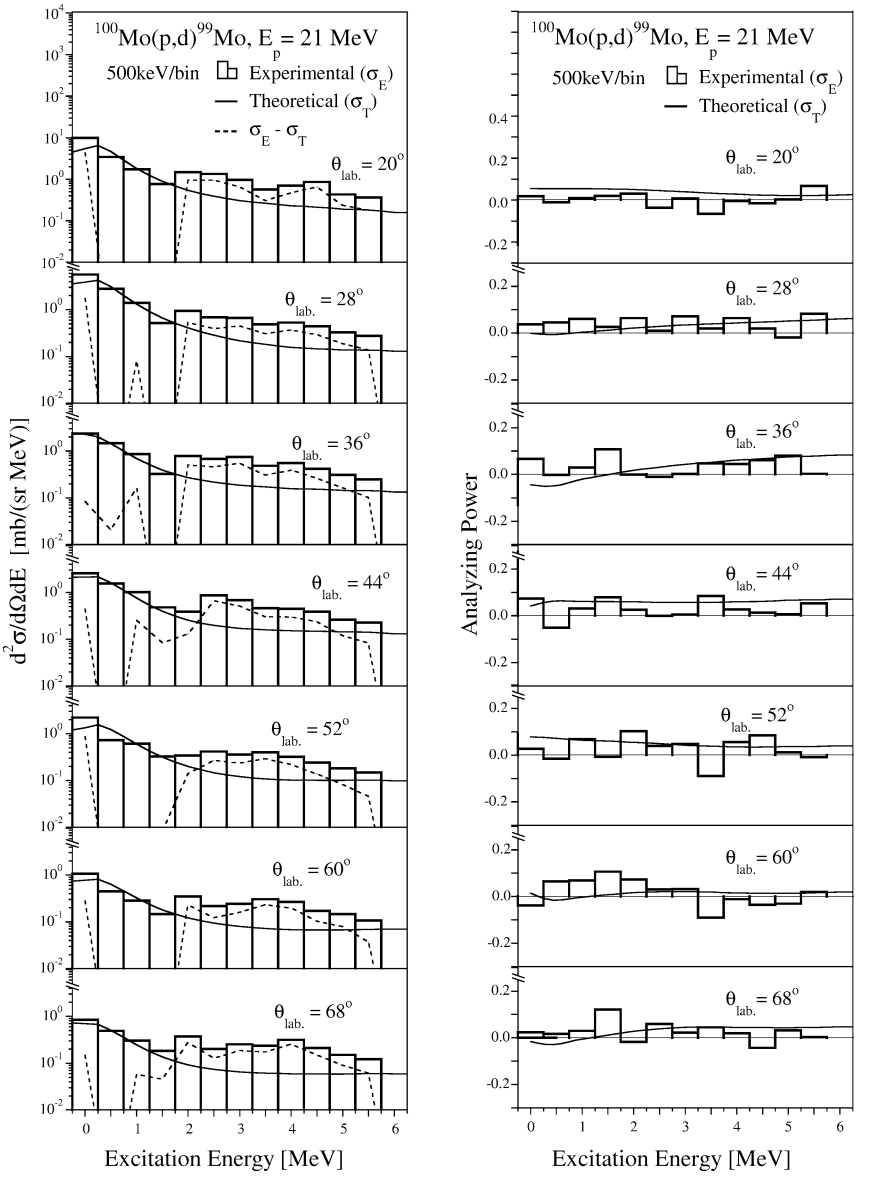

Fig. 10. Double differential energy spectra of cross sections (left) and analyzing powers (right) obtained for the ^{100}Mo$(p, d)^{99}$Mo reaction at 21 MeV.

and continuum-dominated regions. Fig. 11 (bottom) shows a region of 2–2.5 MeV, i.e., the transition area from discrete to continuum regions. It is found from Fig. 11 that the theory is excellent to express the trend of angular distributions of the cross sections and analyzing powers for the 0–2 MeV region, and fairly good for the 2–5.75 MeV region, in

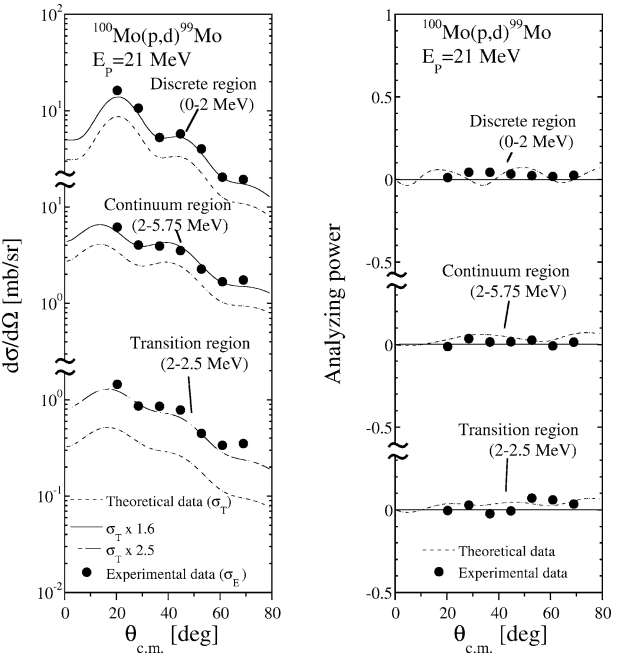

Fig. 11. Angular distributions of the summative cross sections and analyzing powers in the ^{100}Mo$(p,d)^{99}$Mo reaction at 21 MeV. The region 0–2 MeV (top) refers to the discrete peak-dominated area, 2–5.75 MeV (middle) the continuum-dominated area, and 2–2.5 MeV (bottom) the transition area. Dashed curves refer to the predictions due to the present analysis, solid and short-long-lines-dashed curves the predictions after normalized to fit the experimental results. The normalization coefficient is 1.6, 2.5, and 1.6, respectively, for the discrete, transition, and continuum region.

spite of the rough estimation of BCS-theory (Fig. 9) and the overestimation (Fig. 10). As for the absolute value of the cross section, the prediction underestimates the experimental value by a factor of about 1.6 for both the peak- and continuum-dominated regions. As the angular distribution is of forward peak type and underestimated, it is another indication that this contribution is derived from the non-pickup direct reaction process. Since the present theoretical prediction is based on the one-step DWBA model, the fit of the theory to the experiment are quite reasonable.

5. Conclusions

The ^{100}Mo$(p,d)^{99}$Mo reaction has been studied with 21 MeV polarized protons. Angular distributions of the differential cross section and analyzing power have been measured for neutron hole states in ^{99}Mo up to the excitation energy of 5.75 MeV. The data analysis with a standard DWBA theory provides the lj-angular momentum transfers and spectroscopic factors of several excited states up to an excitation energy of 2.921 MeV. The use of a polarized beam improved the results of spin and parity assignments. The wide range of spectra from discrete levels to continuum region have been analyzed consistently

with direct reaction model. The overall hole state strengths are reproduced well using asymmetrical Lorentzian form response functions having energy-dependent spreading widths. The contributions of a non-pickup reaction process are definitely found in the relatively lower excitation energy region.

Acknowledgements

We are grateful to the staff of the Tandem Accelerator Center, University of Tsukuba, for their support during the experiments. One of the authors (Syf) acknowledges the financial support of the Ministry of Education, Science and Culture, Government of Japan, and the leave granted from the National Nuclear Agency of Indonesia (BATAN).

References

[1] M. Sakai, K. Kubo, Nucl. Phys. A 185 (1972) 217.
[2] H. Langevin-Joliot, E. Gerlic, J. Guillot, M. Sakai, J. van de Wiele, A. Devaux, P. Force, G. Lanford, Phys. Lett. B 114 (1982) 103.
[3] M. Matoba, H. Ijiri, H. Kametani, T. Sakae, I. Kumabe, M. Hyakutake, N. Koori, T. Maki, T. Shiba, Phys. Lett. B 149 (1984) 50.
[4] M. Matoba, H. Ijiri, H. Kametani, I. Kumabe, M. Hyakutake, N. Koori, T. Sakae, T. Maki, Nucl. Phys. A 456 (1986) 235.
[5] M. Matoba, H. Ijiri, H. Ohgaki, S. Uehara, T. Fujiki, Y. Uozumi, H. Kugimiya, N. Koori, I. Kumabe, M. Nakano, Phys. Rev. C 39 (1989) 1658.
[6] K. Hisamochi, O. Iwamoto, A. Kisanuki, S. Budihardjo, S. Widodo, A. Nohtomi, Y. Uozumi, T. Sakae, M. Matoba, M. Nakano, T. Maki, S. Matsuki, N. Koori, Nucl. Phys. A 564 (1993) 227.
[7] H. Langevin-Joliot, J. van de Wiele, J. Guillot, E. Gerlic, L.H. Rosier, A. Willis, M. Morlet, G. Duhamel-Chretien, E. Tomasi-Gustafsson, N. Blasi, S. Micheletti, S.Y. van der Werf, Phys. Rev. C 47 (1993) 1571.
[8] M.B. Lewis, Phys. Rev. C 11 (1975) 145.
[9] G.M. Crawley, in: Proceedings of International Symposium on Highly Excited States in Nuclear Reactions, Osaka, 1980, and references therein.
[10] S. Galès, Ch. Stoyanov, A.I. Vdovin, Phys. Rep. 166 (1988) 125, and references therein.
[11] M. Matoba, O. Iwamoto, Y. Uozumi, T. Sakae, N. Koori, H. Ohgaki, H. Kugimiya, H. Ijiri, T. Maki, M. Nakano, Nucl. Phys. A 581 (1995) 21.
[12] M. Matoba, K. Kurohmaru, O. Iwamoto, A. Nohtomi, Y. Uozumi, T. Sakae, N. Koori, H. Ohgaki, H. Ijiri, T. Maki, M. Nakano, H.M. Sen Gupta, Phys. Rev. C 53 (1996) 1792.
[13] Syafarudin, F. Aramaki, G. Wakabayashi, Y. Uozumi, N. Ikeda, M. Matoba, K. Yamaguchi, T. Sakae, N. Koori, T. Maki, in: International Conference on Nuclear Data for Science and Technology, ND2001-conf., 8–11 October, 2001, J. Nucl. Sci. Technol. Suppl. 2 (2002) 377.
[14] S. Aoki, K. Yamaguchi, Syafarudin, G. Wakabayashi, F. Aramaki, Y. Uozumi, A. Nohtomi, T. Sakae, M. Matoba, N. Koori, T. Maki, Y. Tanaka, in: Proceedings of the 1998 Symposium on Nuclear Data, JAERI-conf. 99-002, 1999.
[15] P.K. Bindal, D.H. Youngblood, R.L. Kozub, P.H. Hoffmann-Pinther, Phys. Rev. C 12 (1975) 1826.
[16] R.B. Firestone, V.S. Shirley, C.M. Baglin, S.Y. Frank Chu, J. Zipkin, Table of Isotopes, 8th Edition, Wiley, New York, 1996.
[17] M. Matoba, T. Sakae, T. Yamazaki, S. Morinobu, I. Katayama, M. Fujiwara, Y. Fujita, H. Ikegami, H. Iida, Y. Aoki, Y. Toba, S. Kunori, K. Nagano, K. Hashimoto, K. Yagi, Nucl. Instrum. Methods 196 (1982) 257.
[18] H. Iida, Y. Aoki, K. Yagi, M. Matoba, Nucl. Instrum. Methods 224 (1984) 432.
[19] F.D. Becchetti Jr., G.W. Greenlees, Phys. Rev. 182 (1969) 1190.
[20] P.D. Kunz, code DWUCK, University of Colorado, unpublished.

[21] G.L. Wales, R.C. Johnson, Nucl. Phys. A 274 (1976) 168.
[22] C. Mahaux, R. Sartor, Nucl. Phys. A 493 (1989) 157;
C. Mahaux, R. Sartor, Adv. Nucl. Phys. 20 (1991) 1.
[23] O. Iwamoto, A. Nohtomi, Y. Uozumi, T. Sakae, M. Matoba, M. Nakano, T. Maki, N. Koori, Nucl. Phys. A 576 (1994) 387.
[24] A. Bohr, B.R. Mottelson, in: Nuclear Structure, Vol. I, Benjamin, New York, 1969, Appendix 2D.
[25] G.E. Brown, M. Rho, Nucl. Phys. A 372 (1981) 397.
[26] M. Matoba, O. Iwamoto, Y. Uozumi, T. Sakae, N. Koori, T. Fujiki, H. Ohgaki, H. Ijiri, T. Maki, M. Nakano, Phys. Rev. C 48 (1993) 95.
[27] J.B. French, M.H. Macfarlane, Nucl. Phys. 26 (1961) 168.
[28] Y. Nedjadi, J.R. Rook, Nucl. Phys. A 585 (1995) 641.
[29] P.K.A. de Witt Huberts, J. Phys. G 16 (1990) 507.
[30] A.E.L. Dieperink, P.K.A. de Witt Huberts, Annu. Rev. Nucl. Part Sci. 40 (1990) 239.
[31] M. Matoba, K. Yamaguchi, K. Kurohmaru, O. Iwamoto, S. Widodo, A. Nohtomi, Y. Uozumi, T. Sakae, N. Koori, T. Maki, M. Nakano, Phys. Rev. C 55 (1997) 3152.